Batch and continuous synthesis of well-defined Pt/Al_2O_3 catalysts for the dehydrogenation of homocyclic LOHCs

Yazan Mahayni[a,b], Lukas Maurer[a,b], Ina Baumeister[b], Franziska Auer[a] , Peter Wasserscheid[a,b]
Moritz Wolf[c,*]

[a] Forschungszentrum Jülich GmbH, Helmholtz-Institute Erlangen-Nürnberg for Renewable Energy (IEK-11), Erlangen, Germany

[b] Friedrich-Alexander-Universität Erlangen-Nürnberg (FAU), Lehrstuhl für Chemische Reaktionstechnik, Erlangen, Germany

[c] Karlsruhe Institute of Technology (KIT), Engler-Bunte-Institut & Institute of Catalysis Research and Technology, Karlsruhe, Germany

[*]Corresponding author. Address: Hermann-von-Helmholtz-Platz 1, 76344 Eggenstein-Leopoldshafen,, Germany. E-Mail-address: moritz.wolf@kit.edu

Abstract

The controlled synthesis of supported Pt nanoparticles with well-defined sizes in the range from 1.9 to 6.0 nm and their application in the dehydrogenation of cyclic liquid organic hydrogen carrier (LOHC) molecules are demonstrated. For this purpose, a colloidal approach with a stabilized Pt precursor solution including chemical reduction with aqueous solutions of sodium borohydride ($NaBH_4$) is used. Various synthesis parameters are varied and their effects on the properties of the Pt nanoparticles are studied. Additionally, the nanoparticles were supported on Al_2O_3 powder and the general suitability of the catalysts for the dehydrogenation of the LOHC perhydro benzyltoluene (H12-BT) is demonstrated. The synthesis is then transferred from powder to shaped supports. Moreover, upscaling of the synthesis procedure to 50 g of well-defined catalyst is realized without significant deviations in nanoparticle size but at the expense of a certain activity loss. Finally, a continuous synthesis of Pt/Al_2O_3 catalysts is implemented using a microfluidic reactor. The small-scale, large-scale, and continuous synthesis routes enable the preparation of defined catalysts resulting in a comparable Pt-based productivity in the dehydrogenation of H12-BT.

Keywords

Chemical hydrogen storage; microfluidic synthesis; nanoparticles; platinum; scale-up

Introduction

Numerous studies identified the importance of platinum nanoparticle morphology in a wide variety of heterogeneously catalyzed reactions.[1-6] This also includes the dehydrogenation of cyclic liquid organic hydrogen carriers (LOHCs) using Pt/Al_2O_3 catalysts. For instance, the group of Somorjai intensively studied the structure sensitive behavior of the dehydrogenation of cyclohexane[7-8] and methylcyclohexane (MCH).[9-10] For the dehydrogenation of the LOHC perhydro dibenzyltoluene (H18-DBT), remarkable activity changes were observed by Auer *et al.* for a nanoparticle size range from 1.2 to 4.6 nm. Specific initial productivities of the corresponding catalysts in the dehydrogenation of H18-DBT at 310 °C in the range of 2 to 4 $g_{H2}\ g_{Pt}^{-1}\ min^{-1}$ were reported.[2] This emphasizes the need for scalable synthesis routes for Pt/Al_2O_3 catalysts that allow precise control of the size of the platinum nanoparticles.

Pt/Al_2O_3 catalysts are commonly synthesized via wet impregnation of the support with an aqueous Pt precursor solution.[11-13] This route offers several advantages, such as high dispersion of the metal particles and simple scalability. However, required thermal treatment during subsequent processing of the catalysts *i.e.*, calcination in air at temperatures between 300 and 500 °C[14] or reduction under hydrogen atmosphere at 200 to 600 °C,[15] is associated with challenges. At such elevated temperatures, enhanced particle mobility may result in sintering, which has been observed for thermal treatments under both oxidative[16-19] and H_2-containing[20-21] environment. These effects may alter the morphology of the Pt nanoparticles and hence the specific catalytic activity in structure sensitive dehydrogenation reactions. Contrary, direct chemical reduction to metallic Pt can circumvent thermal treatment prior to catalytic application. For example, sodium borohydride ($NaBH_4$) has been widely employed as a reducing agent for the colloidal synthesis of transition metals.[22-30] Moreover, chemical reduction has proven to yield well-defined Pt nanoparticles with distinct control over particle size in combination with a narrow particle size distribution.[22-25] This is due to the adjustable amount of the liquid reducing agent and thus the strength and speed of the reduction compared to alternative methods *e.g.*, with gaseous H_2. In addition, the utilization of steric capping agents, such as polyvinylpyrrolidone (PVP), is essential to circumvent agglomeration of the synthesized nanoparticles.[31-32] For catalytic applications, the separately synthesized, chemically reduced nanoparticles can be immobilized onto a support.

In this work, we study the influence of the synthesis parameters on the size of nanoparticles in Pt/Al_2O_3 catalysts obtained via the colloidal synthesis with chemical reduction and subsequent immobilization onto the support. Aside from catalytic testing in the dehydrogenation of H18-

DBT, the transferability of the synthesis route from powder to shaped Al_2O_3 supports is studied as the latter are required for state-of-the-art commercial LOHC dehydrogenation reactors.[33-34] To overcome mass transfer limitations, egg-shell catalysts are used in the dehydrogenation of homocyclic LOHCs, such as perhydro dibenzyltoluene[35-36] and perhydro benzyltoluene.[37-38] Lastly, we describe the scale-up of the colloidal synthesis to a fivefold batch size to produce 50 g of shaped Pt/Al_2O_3 egg-shell catalysts with well-defined nanoparticle size. Additionally, the synthesis process is transferred from batch to continuous operation to enable large-scale catalyst production in the absence of thermal processing.

Methodology

Catalyst synthesis

The supported Pt nanoparticle catalysts were synthesized by modifying procedures (Figure 1) described in literature.[23, 39] At first, the capping agent polyvinylpyrrolidone (PVP, MW 40 000, Sigma Aldrich) was dissolved in 50 mL of Millipore water and ultra-sonicated for 15 min. An amount of 52 mg of chloroplatinic acid (H_2PtCl_6, Sigma Aldrich) was added to the PVP solution followed by ultra-sonication for 1 min. The obtained solution (pH ~ 2.5) was magnetically stirred at 1500 rpm before rapid injection of the reducing agent. Chemical reduction was induced through the addition of an aqueous solution of sodium borohydride ($NaBH_4$, 33mM in Millipore Water, Acros Organics), which demonstrated a pH ~ 10 and was cooled in an ice bath to limit decomposition of $NaBH_4$ via hydrolysis (Figure S1).[40-42] Different volumes of $NaBH_4$ solution were added (0.2-2.4 mL) to yield various sizes of the Pt nanoparticles. After 1 min of stirring, the nanoparticles were immobilized onto an Al_2O_3 powder (PURALOX TH100/150, Sasol Germany) or on shaped Al_2O_3 tablets (hollow cylinders with L x D_{out} x D_{in}: 5.0 x 5.0 x 2.2 mm, Sasol Germany) and left overnight under moderate stirring to ensure homogeneous distribution of the nanoparticles on the support. A loading of 0.2 wt% Pt was targeted for all catalysts by the addition of the appropriate amount of alumina support (typically 10 g). Finally, the solvent was evaporated at 80 °C and 250 mbar in a rotary evaporator to obtain the catalyst for analysis and catalytic testing without further treatment. Modified procedures deviating from this standardized method, such as a continuous microfluidic synthesis (Figure 1), are described in the manuscript where applicable.

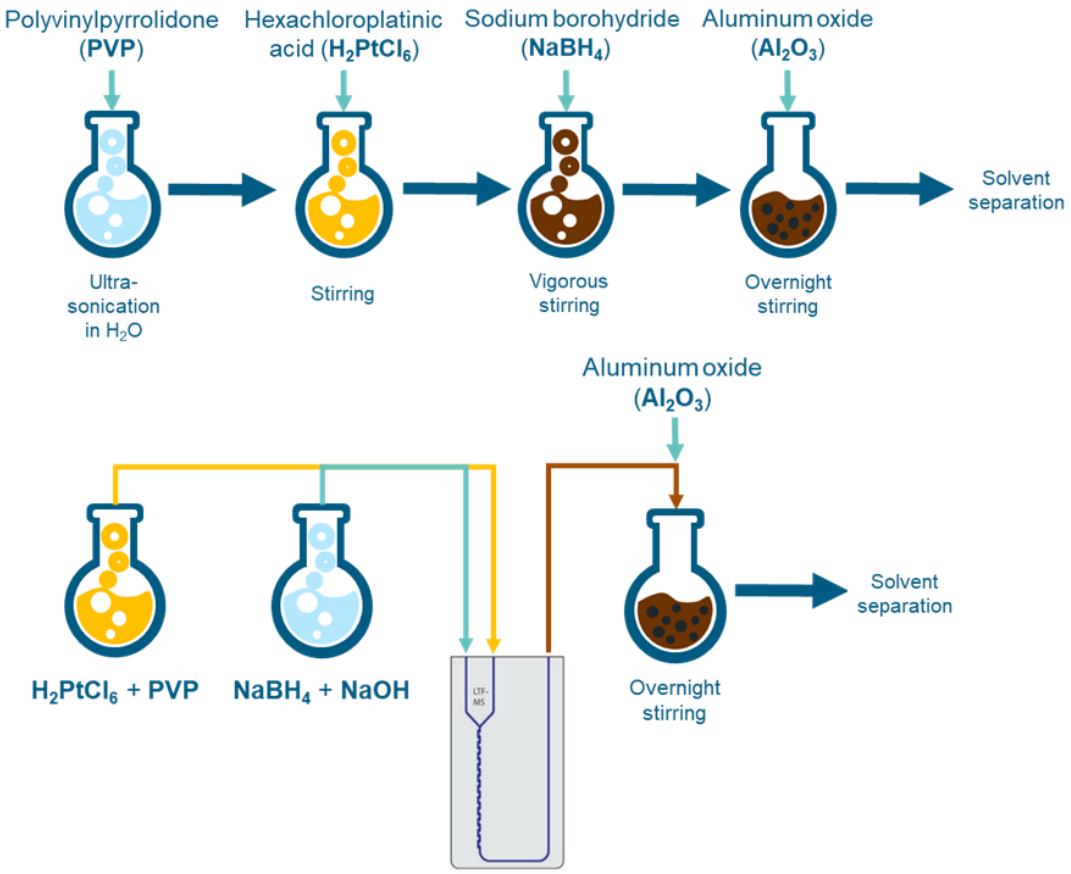

Figure 1: Batch synthesis route of Pt/Al_2O_3 catalysts via the colloidal approach (top). Continuous synthesis route of Pt/Al_2O_3 catalysts via a microreactor and by the colloidal approach (bottom).

Material characterization

N_2 physisorption was conducted in a Tristar II Plus (Micromeritics). The samples were degassed at 250 °C and 0.01 mbar under a flow of He. The evaluation of the textural properties of the support material was analysed via the BET method in the relative pressure range 0.05-0.35. The BJH method was applied to obtain pore characteristics.

X-ray diffraction patterns were recorded with an X-Pert Pro (Malvern Panalytical) equipped with an X'Celerator detector in a 2θ range from 10° to 90° (step size of 0.015°, exposure time of 0.75 s, X-ray source with $\lambda_{Cu,K\alpha1}$ = 1.54056 Å). The powder sample was compressed in a sample holder and the surface was flattened before the measurement. The data was processed with X'Pert Highscore Plus and compared with simulated reflections from the Inorganic Crystal Structure Database (ICSD).

Pt loadings of the catalysts were analysed by means of inductively coupled plasma optical emission spectroscopy (ICP-OES) using a Ciros CCD device (Spectro Analytical Instruments GmbH). The solid samples were dissolved using a concentrated $HCl:HNO_3:HF$ mixture with a

3:1:1 volumetric ratio and microwave digestion. The instrument was calibrated with standard solutions of Pt prior to the measurements.

High-resolution transmission electron microscopy (HR-TEM) was conducted for size analysis of the supported Pt nanoparticles in a CM30 (Philips). For sample preparation, small amounts of the Pt/Al_2O_3 catalysts were dispersed in ethanol and drop-casted on 300 mesh copper grids with lacey carbon coating (Plano GmbH). The size of 150-400 Pt nanoparticles from different areas of the sample were analysed individually by two operators using ImageJ to obtain size distributions.[43]

CO pulse chemisorption was used to probe the accessible active sites of the supported nanoparticles. For this, a total of 300 mg of the respective Pt/Al_2O_3 catalyst materials were analysed in an Autochem II 2920 (Micromeritics). The samples were flushed by a continuous flow of 20 mL min^{-1} He with intermittent dosing of 368 µL CO to quantify the amount of adsorbed CO.

Dehydrogenation of H12-BT

All dehydrogenation experiments in this work were conducted in a 100 mL three-neck round-bottom flask.[13] H12-BT (degree of hydrogenation >97.5%; Hydrogenious LOHC Technologies GmbH) was weighed into the flask. Hereafter, a thermocouple immersed in the liquid, a catalyst dosing device and an Ar inlet line were connected through the side necks, while an intensive condenser was attached to the middle-neck.[13] The corresponding amount of catalyst material to realize a Pt:H12-BT ratio of 0.1 mol% was loaded into the dosing device. Before the start of the experiments, an Ar flow of 300 mL min^{-1} was set by a mass-flow controller (Bronkhorst Deutschland Nord GmbH). The system was then heated to the desired reaction temperature of 250 °C by a heating jacket with a temperature controller. The catalyst was released into the pre-heated liquid phase upon stabilization of the temperature to initiate the reaction. To quantify the amount of released H_2, a thermal conductivity detector (TCD, Messkonzept GmbH) was used to analyse the concentration of H_2 in the off gas at an internal set temperature of 60 °C. From the TCD measurement, the volumetric flow rate of hydrogen $\dot{V}_{H_2}$ can be calculated using Equation (1).[13]

$$\dot{V}_{H_2} = \frac{\varphi_{H_2}}{1 - \varphi_{H_2}} \cdot \dot{V}_{Ar} \quad (1)$$

Where φ_{H_2} stands for the measured volume fraction of hydrogen in the exhaust gas stream and $\dot{V}_{Ar}$ for the volumetric flow of argon with which the reaction chamber is overflown. The productivity *P* of the catalyst can then be calculated using the volumetric flow rate of hydrogen according to Equation (2).[13]

$$P = \frac{\dot{V}_{H_2} \cdot \rho_{H_2}}{m_{cat} \cdot w_{Pt}} \quad (2)$$

Where the density of hydrogen at 273.15 K ($\rho_{H_2} = 0.0899$ kg/m^3), the catalyst mass m_{cat} and the metal loading w_{Pt}, measured by ICP, were used for the calculation.

In addition, the degree of dehydrogenation (DoDH) can be derived with the know amount of maximum reversibly bound H_2 in H12-BT $n_{H2,max}$ according to Equations (3) and (4).[13]

$$n_{H_2}(t) = \int_0^t X_{\frac{H_2}{Ar}} \cdot \dot{V}_{Ar} \cdot \frac{\rho_{H_2}}{M_{H_2}}\, dt \quad (3)$$

$$DoDH = \frac{n_{H_2}(t)}{n_{H_2,max}} \quad (4)$$

Results and discussion

Based on previous works by Auer *et al.*[2], the selected Al_2O_3 powder support provides suitable properties for the dehydrogenation of homocyclic LOHC compounds *e.g.*, H18-DBT or H12-BT. XRD analysis of the powder support reveals a γ-Al_2O_3 structure (Figure S2 in the supplementary information). A specific surface area of 162 m^2 g^{-1} and a mean pore diameter of 20 nm were determined by means of N_2 physisorption (Table 1, Figure S3). A sufficiently large specific surface area allows for a good dispersion of the platinum nanoparticles on the support with large inter-particle distances, whereas a large mean pore diameter minimizes mass transport limitations due to the bulky LOHC molecules.[19]

Table 1: Morphology of powder and shaped Al_2O_3 supports.

Support	Surface area / m^2 g^{-1}	Mean pore diameter / nm	Size
Powder[a]	162	20	35 µm (d_{50})
Shaped[44]	180	n.a.	5.0 x 5.0 x 2.2 mm (L x D_{out} x D_{in})

[a] As determined by means of N_2 physisorption

For a first conceptual test, a Pt/Al_2O_3 catalyst was prepared based on the synthesis described in the methodology section and found in Figure . Colloidal Pt nanoparticles were synthesized using a PVP:Pt ratio of 10:1 and a $NaBH_4$:Pt ratio of 0.31 mol_{NaBH4} mol_{Pt}^{-1} based on literature.[2, 23, 39] A 0.20 wt.% Pt/Al_2O_3 catalyst was targeted by immediate immobilization of the nanoparticles onto the powder Al_2O_3 support. An actual Pt loading of 0.18 wt.% was determined by means of ICP-OES. Nanoparticle size analysis using high-resolution transmission electron microscopy (HR-TEM) resulted in a mean diameter of 2.1 nm (Figure 2a).

The catalyst was then tested in the dehydrogenation of H12-BT at 250 °C to assess the general suitability of chemical reduction of the catalyst during colloidal synthesis for subsequent catalytic applications. The Al_2O_3 support does not provide any dehydrogenation activity (Figure S4). The observed initial productivity of the synthesized Pt/Al_2O_3 catalyst of up to 0.5 g_{H2} g_{Pt}^{-1} min^{-1} (Figure 2b) during batch dehydrogenation is comparable with reported values of 0.7 to 0.9 g_{H2} g_{Pt}^{-1} min^{-1} by Rüde *et al.*[38], who tested a commercial, selectively poisoned catalyst at significantly higher temperature of 290 °C.

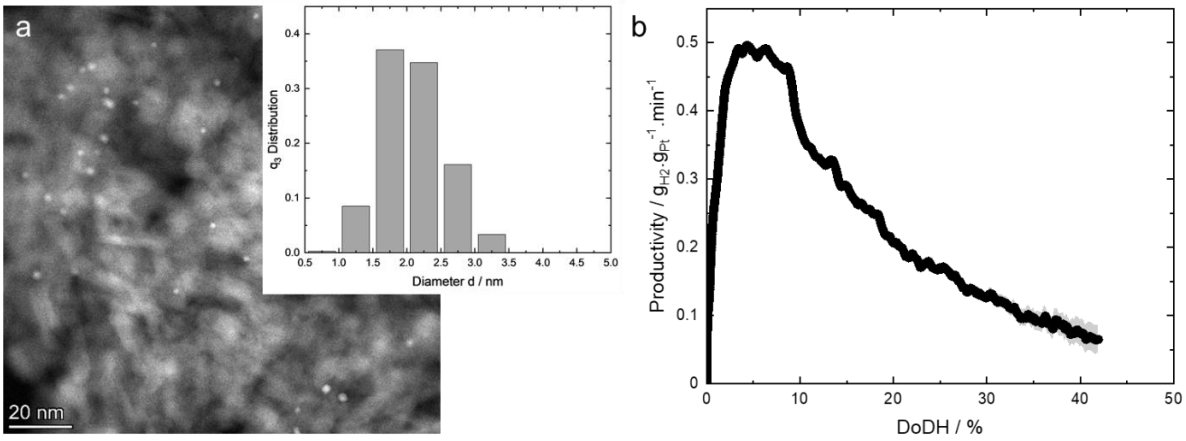

Figure 2: (a) HR-TEM micrograph and particle size distribution of colloidal, chemically reduced Pt nanoparticles immobilized onto a powder Al_2O_3 support and (b) productivity as a function of degree of dehydrogenation (DoDH) during semi-batch dehydrogenation of H12-BT. The shaded data resembles the deviation during reproduced performance testing. Reaction conditions: T = 250 °C, Pt:LOHC = 0.001 mol_{Pt} mol_{LOHC}^{-1}, F_{Ar} = 300 mL min^{-1}, $t_{Reaction}$ = 120 min, Pt loading = 0.2 wt.% Synthesis conditions: Batch procedure with powder Al_2O_3 support, PVP:Pt = 10 g_{PVP} g_{Pt}^{-1}, $NaBH_4$:Pt = 0.31 mol_{NaBH4} mol_{Pt}^{-1}.

The successful dehydrogenation of H12-BT demonstrates the catalytic activity of the immobilized, chemically reduced nanoparticles. These nanoparticles are deployed without any pre-treatment e.g., calcination or reduction in O_2-rich or H_2-rich atmospheres,

respectively, and are stabilized by the capping agent PVP. The steric and bulky PVP molecule limits the growth of the nanoparticles after the addition of $NaBH_4$ which itself instantly triggers the nucleation of Pt monomers and at some point, the growth of the present nanoparticles. This is accompanied by a change of colour from yellow (Pt-precursor + PVP) to brown (after $NaBH_4$ addition), which remains unchanged until the solvent removal step. This, at least visually, indicates that PVP stabilizes the morphology of the formed Pt nanoparticles and is discussed in more detail in the following section of this manuscript. The Pt nanoparticles are physically immobilized on the Al_2O_3 support during solvent removal for the synthesis route of this manuscript, contrary to wet impregnation routes, where the support surface is modified with a Pt precursor and then thermally reduced to metallic Pt nanoparticles. [11-13]

Pt nanoparticle size control in batch procedure

First, the influence of the gravimetric ratio of PVP:Pt on the nanoparticle size in the respective catalysts was evaluated. However, no significant change in the resulting Pt nanoparticle size of 2.2 nm was observed in the range of 5:1 to 15:1 (Figure 3). Only the highest ratio of 20:1 resulted in larger nanoparticles, but reproducible syntheses become challenging, most likely due to an insufficient control of the particle growth. Since the large PVP molecules (40,000 g mol^{-1}) may prevent access to the Pt surface, the accessibility of the metallic Pt sites was probed for different PVP:Pt ratios by means of CO pulse chemisorption (Figure 3). A detrimental influence of surfactants on catalysis has previously been reported,[45-46] which renders synthesis routes with low to zero amount of surfactants highly desirable.[47] Low PVP:Pt ratios result in a specific adsorption of CO of approx. 10 µmol g^{-1}, which is close to the expected amount for fully accessible spherical 2.2 nm nanoparticles (13.3 µmol g^{-1}). This result also suggests that the approximation of the nanoparticle size based on HR-TEM analysis is applicable for the herein studied materials. Interestingly, the amount of adsorbed CO decreases below 4 µmol g^{-1} when increasing the PVP:Pt ratio to 15 g_{PVP} g_{Pt}^{-1}. This indicates blockage of Pt surface by the bulky stabilizer at PVP:Pt ratios ≥15. As the CO adsorption capacity is comparable for the lower ratios of 5 and 10 g_{PVP} g_{Pt}^{-1}, no significant hindrance is expected for these low PVP:Pt ratios and 5 g_{PVP} g_{Pt}^{-1} was selected for subsequent catalysts syntheses.

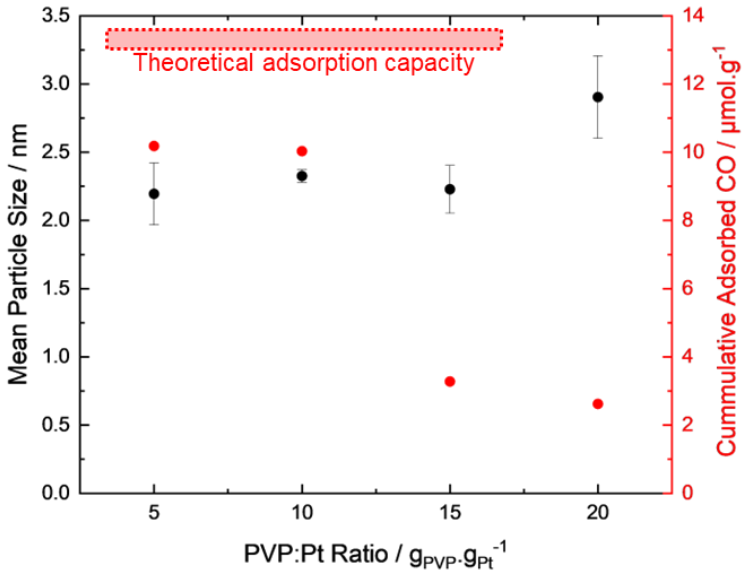

Figure 3: Influence of the specific amount of capping agent PVP on the size of synthesized Pt nanoparticles in the catalysts according to HR-TEM analysis and the cumulative amount of adsorbed CO. Red box indicates the approximated CO adsorption capacity for the smaller nanoparticle sizes for spherical nanoparticles with full accessibility of the Pt surface. Synthesis conditions: Batch procedure with $NaBH_4$:Pt ratio = 0.31 mol_{NaBH4} mol_{Pt}^{-1}. Error bars represent the standard deviation of the mean nanoparticle sizes from three reproductions of each synthesis.

Analogous to the previous experiments with varying amounts of capping agent, the influence of the amount of reducing agent was also studied. Since the degree of reduction is linked to the utilized amounts of reducing agent and metal precursor, the molar $NaBH_4$:Pt ratio is herewith considered. This ratio is systematically varied in the range of 0.21 to 0.47 mol_{NaBH4} mol_{Pt}^{-1}. Size analysis of the platinum nanoparticles in the catalysts was, once again obtained, based on HR-TEM analysis since CO chemisorption proved to be affected by the presence of PVP (Figure 3). While a strong effect for high PVP:Pt ratios was clearly identified, a less pronounced effect at low ratios cannot be fully excluded. Further, the size distribution can only be analyzed by means of HR-TEM. Such a size analysis is associated with certain errors stemming from setting the focus, hindered analysis due to the Al_2O_3 support, individual perception of the operator etc. Hence, we conducted three repetitions of the synthesis with individual size analyses to increase the significance of the results.

Expectedly and in agreement with the model of particle formation proposed by LaMer *et al.*[48], the platinum nanoparticle size strongly depends on the amount of $NaBH_4$ used for the reduction (Figure 4). Increased $NaBH_4$:Pt ratios result in a higher monomer concentration and, consequently, a faster nucleation rate. Hence, the monomer concentration remains beyond the critical supersaturation for longer durations, enriching the particle nucleation regime.

Nevertheless, if the $NaBH_4$:Pt ratio is further increased, the size of randomly formed clusters increases due to the prompt monomer formation. This induces the formation of larger nuclei that contribute to a rapid drop in monomer concentration below the critical supersaturation *i.e.*, terminating the nucleation regime and initiating particle growth.[49] Moreover, rapid reduction in the case of the highest $NaBH_4$:Pt ratio may cause the formation of inhomogeneities within the suspension, which leads to a broadening of the particle size distribution and lower reproducibility. A similar correlation between the applied $NaBH_4$:Pt ratio and the resulting size of PVP protected nanoparticles is described by Bedia *et al.*[50] Overall, an increase of the $NaBH_4$:Pt ratio leads to an increase in the nanoparticle size covering a size range from 2 to 6 nm. All $NaBH_4$ solutions were diluted, which generally facilitates the synthesis of small well-defined nanoparticles with narrow size distributions. This is again in agreement with LaMer *et al.*[48]

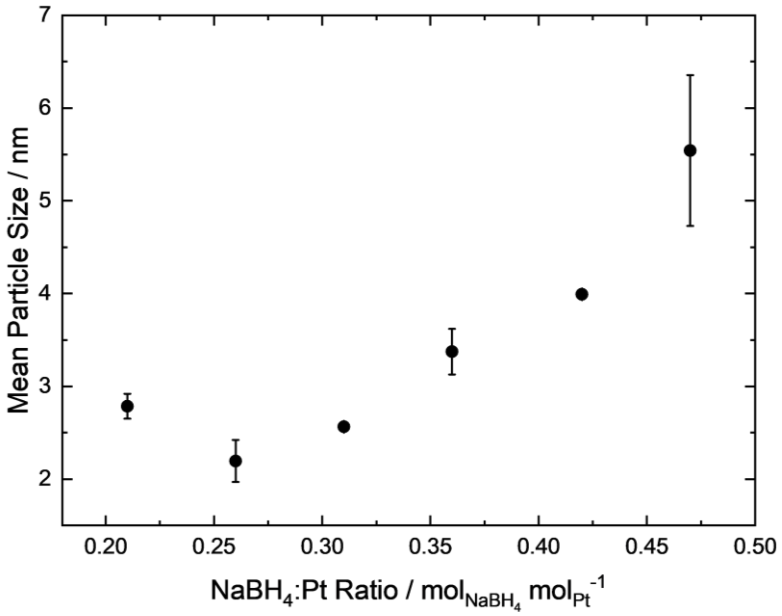

Figure 4: Influence of the specific amount of aqueous reducing agent $NaBH_4$ on the size of synthesized platinum nanoparticles according to HR-TEM analysis. Synthesis conditions: Batch procedure with PVP:Pt ratio = 5 $g_{PVP}\ g_{Pt}^{-1}$. Error bars represent the standard deviation of the average value over three reproductions.

Two exemplary HR-TEM micrographs and the corresponding narrow particle size distributions of catalysts synthesized with $NaBH_4$:Pt ratios of 0.21 and 0.47 $mol_{NaBH4}\ mol_{Pt}^{-1}$ are shown in Figure 5, while the analysis of the remaining catalysts can be found in the supplementary information (Figures S5 & S6). In contrast to the general trend, the lowest $NaBH_4$:Pt ratio resulted in the formation of slightly enlarged nanoparticles (Figure 4). This may be due to the weak reduction force of the diluted reducing agent, which results in a slow formation of metal monomers. Accordingly, the nucleation rate is similarly slow. This is due to the consumption

of the slowly formed Pt monomers during the nucleation phase, which results in a quick drop in monomer concentration shortly after exceeding the critical supersaturation. During the following growth regime, the ongoing reduction of platinum mostly contributes to particle growth rather than to the formation of new nuclei.

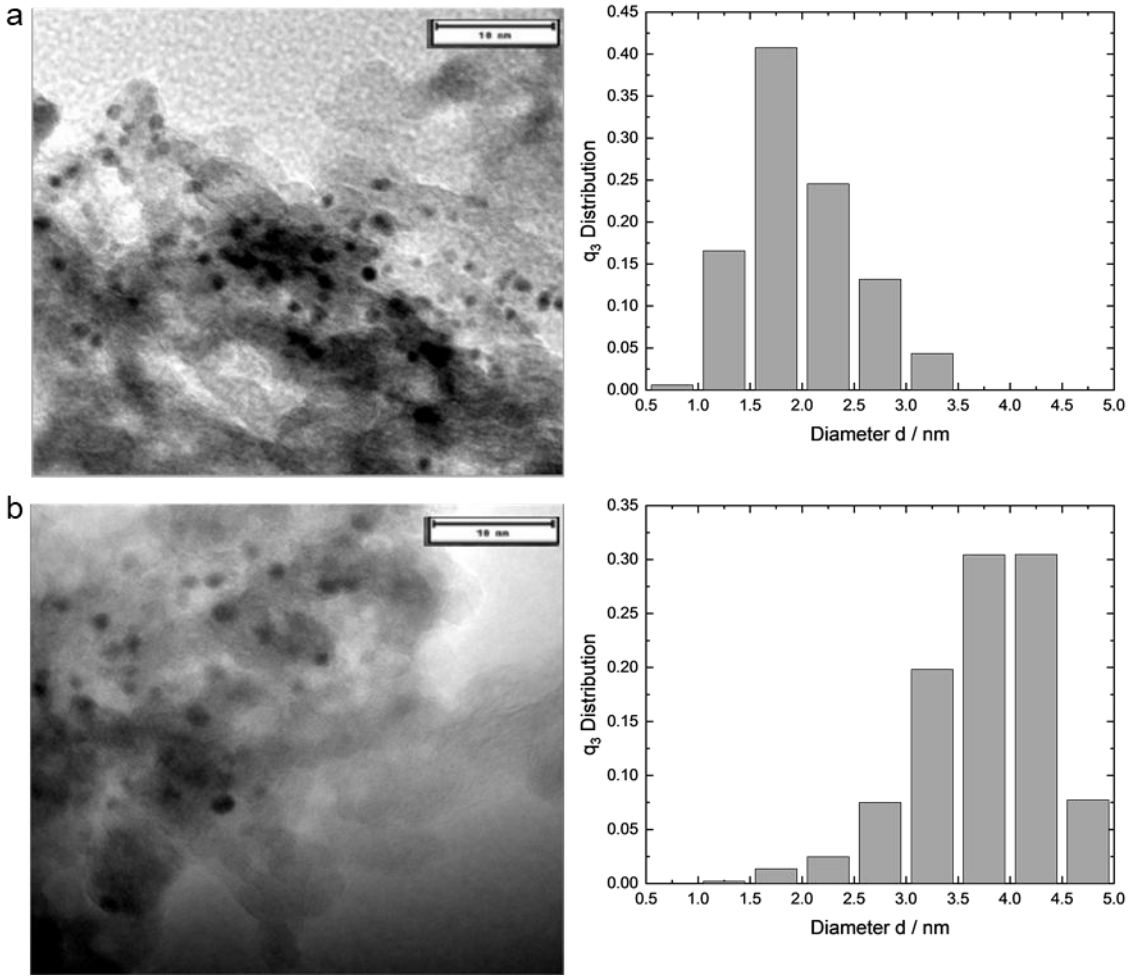

Figure 5: HR-TEM micrographs (scale bars: 10 nm) and Pt nanoparticle size distributions for Pt/Al_2O_3 catalysts synthesized with $NaBH_4$:Pt ratios of (a) 0.26 and (b) 0.47 mol_{NaBH4} mol_{Pt}^{-1} resulting in mean platinum particle sizes of 2.0 and 4.7 nm, respectively. Synthesis conditions: Batch procedure with PVP:Pt ratio = 5 g_{PVP} g_{Pt}^{-1}.

For the following catalyst syntheses, a $NaBH_4$:Pt ratio of 0.31 mol_{NaBH4} mol_{Pt}^{-1} was selected as the obtained particle size is sufficiently small to enable high Pt dispersions and in combination with a high reproducibility.

Immobilization of Pt nanoparticles onto shaped supports

Commonly, Pt/Al_2O_3 shaped catalysts for the dehydrogenation of H18-DBT and H12-BT are synthesized via wet impregnation.[35] Strong interaction via electrostatic adsorption enables

high dispersions and allows for the desired egg-shell distribution of the active component and also determine the nanoparticle size or even shape.[11, 51] Herein, the separate synthesis with subsequent immobilization of nanoparticles onto a support material preserves their well-defined structure, while an appropriate distribution of the well-defined nanoparticles on the support material may be challenging. This is evidenced for different shaped catalyst batches using the previously described batch nanoparticle synthesis with subsequent immobilization onto the support, which exhibit apparent inhomogeneities for a shaped support (Figure S7). To accommodate immobilization onto shaped supports, the drying procedure in a rotary evaporator was divided into two sections: slow nanoparticle deposition at a moderate pressure of 250 mbar, followed by solvent evaporation at 35 mbar combined with a faster rotation of the synthesis flask (150 vs. 50 rpm). This procedure facilitated the penetration of the outer layers of the shaped support by dispersed nanoparticles, which already contain immobilized Pt nanoparticles. The homogeneity of the obtained shaped catalyst was thereby significantly improved (Figure 6).

Figure 6: Photograph of four batches of synthesized Pt/Al_2O_3 with optimized immobilization procedure of chemically reduced colloidal nanoparticles onto hollow cylinders. Synthesis conditions: Batch procedure, PVP:Pt ratio = 5 g_{PVP} g_{Pt}^{-1} and $NaBH_4$:Pt ratio = 0.31 mol_{NaBH4} mol_{Pt}^{-1}.

To evaluate the performance of the shaped catalysts in the dehydrogenation of H12-BT, Pt nanoparticles with an average diameter of 2.3 nm were synthesized and immobilized onto Al_2O_3 support material, both as powder and hollow cylinders. The catalytic testing was performed in a semi-batch dehydrogenation experiment at 250 °C (Figure 7). The initial productivity of the shaped catalysts was slightly reduced, while H_2 release at higher DoDH was facilitated resulting in comparable DoDHs of 42% and 46% after 120 min for the powder and shaped catalysts, respectively. The initial divergence may be caused by mass transport limitations in case of the shaped catalyst, as large amounts of gaseous H_2 are released during

this initial phase of the semi-batch dehydrogenation. However, this effect is not very pronounced due to the low egg-shell thickness. Peters *et al.*[52] studied the macrokinetic effects in perhydro-N-ethylcarbazole (H12-NEC) dehydrogenation by using egg-shell catalysts with various shell thicknesses. Based on their findings for H12-NEC, the absence of mass transport limitations for a reaction at 250 °C with a catalyst of approximately 5 µm shell thickness can be assumed.

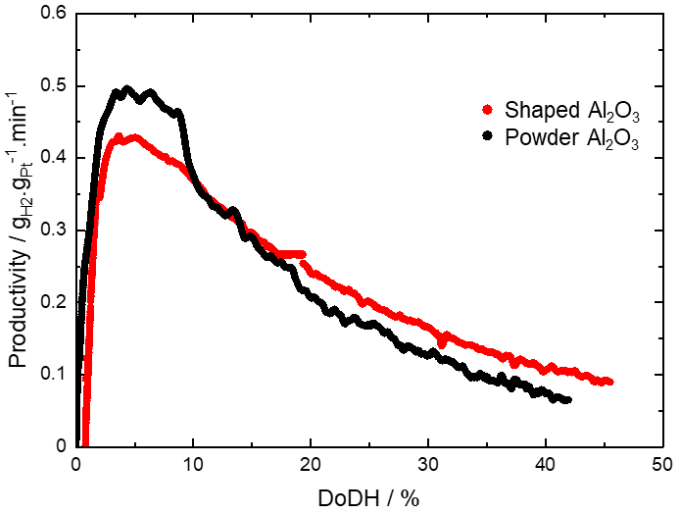

Figure 7: Productivity of Pt as a function of the degree of dehydrogenation (DoDH) for synthesized Pt/Al_2O_3 powder and shaped catalysts with Pt nanoparticle sizes of 2.3 nm during semi-batch dehydrogenation of H12-BT. Reaction conditions: T = 250 °C, $m_{Catalyst}$= 10 g, Pt:LOHC = 0.001 mol_{Pt} mol_{LOHC}^{-1}, F_{Ar} = 300 mL min^{-1}, $t_{Reaction}$ = 120 min, Pt loading = 0.2 wt.%. Synthesis conditions: Batch procedure with PVP:Pt ratio = 5 g_{PVP} g_{Pt}^{-1}, $NaBH_4$:Pt ratio = 0.31 mol_{NaBH4} mol_{Pt}^{-1}.

To further investigate the scalability of the presented colloidal approach, a fivefold scale-up of the batch synthesis of well-defined platinum nanoparticles with a mean particle size of 2.3 nm with subsequent immobilization onto shaped alumina yielding 50 g of Pt/Al_2O_3 catalysts in one step was conducted. However, the scale-up resulted in a worse performance during dehydrogenation of H12-BT at 250 °C (Figure 8) when compared to the catalyst synthesized on a small scale with a total amount of 10 g. This may be caused by an inferior nanoparticle deposition with potential agglomeration and/or low inter-particle distances. With further optimization of the deposition procedure, the performance loss of the large-scale synthesis using shaped supports may be minimized.

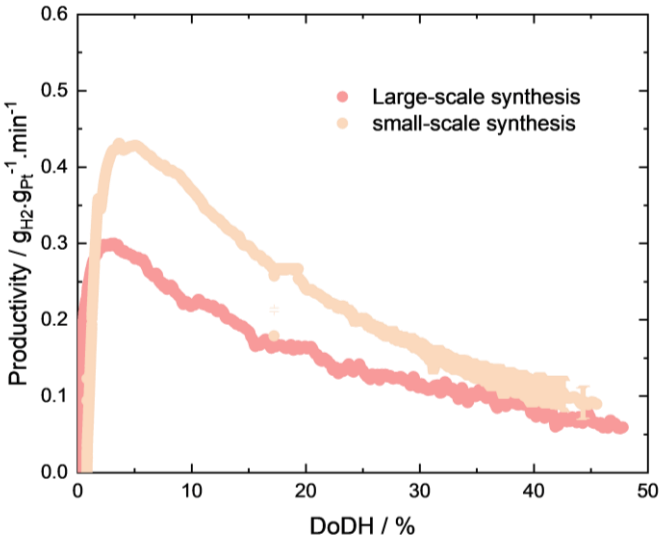

Figure 8: Productivity of Pt as a function of the degree of dehydrogenation (DoDH) during semi-batch dehydrogenation of H12-BT using the fivefold Pt/Al_2O_3 shaped catalyst compared to the small-scale synthesis. Reaction conditions: T = 250 °C, Pt:LOHC = 0.001 mol_{Pt} mol_{LOHC}^{-1}, F_{Ar} = 300 mL min^{-1}, $t_{Reaction}$ = 120 min, Pt loading = 0.2 wt.%. Synthesis conditions: Batch procedure with PVP:Pt ratio = 5 g_{PVP} g_{Pt}^{-1}, $NaBH_4$:Pt ratio = 0.31 mol_{NaBH4} mol_{Pt}^{-1}.

The reproducibility of the performance of different samples within the same batch of shaped catalysts synthesized on the large scale was also demonstrated (Figure S8). Moreover, the platinum loading according to ICP-OES analysis was consistent for several independent cylinders from the large-scale catalyst batch (Table S1). This illustrates the scalability and reproducibility of the colloidal approach, especially for shaped catalysts. The optimized solvent separation procedure thereby enables an enhanced distribution of the platinum nanoparticles on the support material and batch homogeneity.

Continuous Synthesis

With regard to a further upscaling of the synthesis of well-defined Pt nanoparticles, especially with respect to the production of larger catalyst quantities for use in technical reactors, a continuous nanoparticle synthesis is of special interest. Here, the long-term stability of the reducing agent is of great importance as it is not consumed immediately. In literature, stabilization of the reducing agent $NaBH_4$ by NaOH has been ascribed to the pH dependency of its hydrolysis (Figure S1). A larger pH value preserves its reducing ability, and thus affects particle formation. Usually, a pH of 12 is targeted as the half-life of the reducing agent increases from 9.1 min (aqueous solution at pH 10) to 6.3 days (pH 12).[53-56]

At first, the role of pH adjustment during the synthesis of nanoparticles with narrow size distributions over an extended particle size range was examined. Various amounts of $NaBH_4$

were dissolved in 10 mM NaOH solution (pH 12) and used for the synthesis of Pt nanoparticles. The modification of the batch synthesis with stabilized reducing agent resulted in a particle size range of 1.8 to 2.8 nm (Figure 9), which is smaller than without the use of NaOH. However, the control of the final particle size increases drastically.

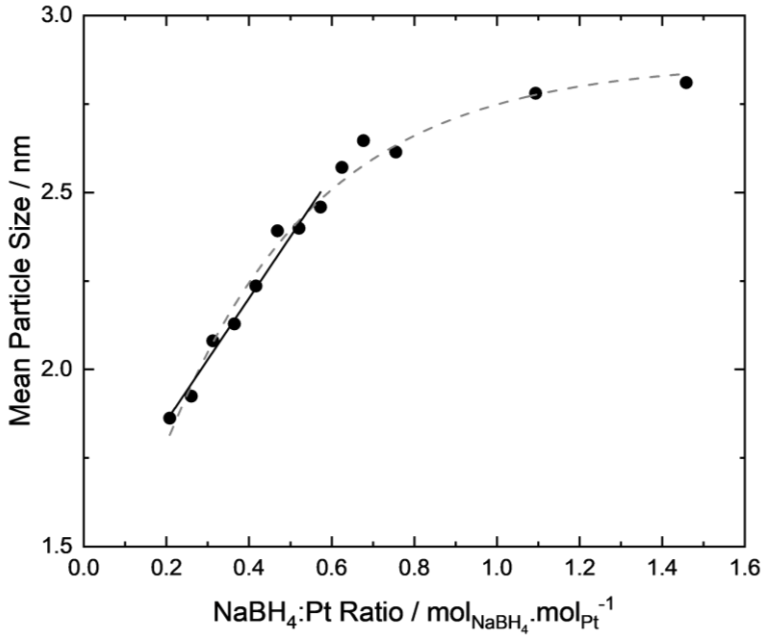

Figure 9: Influence of the specific amount of basic reducing agent $NaBH_4$ on the size of Pt nanoparticles according to HR-TEM analysis. Synthesis conditions: Batch procedure with Al_2O_3 powder, PVP:Pt ratio = 5 $g_{PVP}\,g_{Pt}^{-1}$, c_{NaOH} = 10 mM. Dashed line represents exponential fit of the whole range. Solid line represents linear fit according to Equation (5).

For $NaBH_4$:Pt ratios exceeding 0.7 $mol_{NaBH4}\ mol_{Pt}^{-1}$, the obtained Pt nanoparticle sizes increase only marginally with increasing $NaBH_4$:Pt ratio and strive towards a plateau of a maximum nanoparticle size of 2.8 nm. This threshold was also observed by Van Rheenen *et al.*[54] using a significantly higher $NaBH_4$:Pt ratio of 18.3 $mol_{NaBH4}\ mol_{Pt}^{-1}$, suggesting 2.8 nm as the maximum achievable particle size in the applied colloidal synthesis with basic $NaBH_4$ solutions at pH 12 under ambient conditions. Within the range of 0.2 to 0.7 $mol_{NaBH4}\ mol_{Pt}^{-1}$, the mean Pt nanoparticle sizes exhibit a linear dependency with respect to the $NaBH_4$:Pt ratio. These findings emphasize the importance of a consistent and controllable reduction force for a highly size-selective synthesis of Pt nanoparticles. The linear correlation in the mentioned range (0.2 to 0.7 $mol_{NaBH4}\ mol_{Pt}^{-1}$) may be described by Equation (5).

$$d_v = \left(1.73 \cdot \left(\frac{n_{\mathrm{NaBH_4}}}{n_{\mathrm{Pt}}}\right) + 1.51\right) \mathrm{nm} \tag{5}$$

The results of the synthesis using basic $NaBH_4$ solutions are compared to the previously demonstrated correlation using aqueous $NaBH_4$ solutions (Figure S9). Here, Pt nanoparticles

synthesized via basic $NaBH_4$ demonstrate smaller particle sizes for the same $NaBH_4$:Pt ratio. It is also noteworthy that these nanoparticle sizes are less sensitive to the concentration of reducing agent than in the previously synthesized catalysts using aqueous $NaBH_4$ solutions. This, and the maximum achievable particle size at 2.8 nm, is a clear indication for a successful inhibition of the hydrolysis of $NaBH_4$ in NaOH, when compared to the rash hydrolysis in aqueous solutions. This allows better control over the particle's reduction. Based on these results, a foundation for the controlled synthesis of well-defined Pt nanoparticles is established where Pt/Al_2O_3 catalysts with platinum particle sizes of 1.9-6.0 nm may be synthesized using aqueous $NaBH_4$ solutions, as well as 1.8-2.8 nm via basic $NaBH_4$ solutions, with the latter demonstrating better control and reproducibility of particle size.

With the successful stabilization of the reducing agent, a continuous synthesis of well-defined Pt nanoparticles can be implemented. Therefore, a microfluidic reactor (R-01) in combination with a two-channel syringe pump (P-01) was developed. The two stock solutions (aqueous Pt-PVP and NaOH stabilized $NaBH_4$ solutions) are provided in separate syringes (B-01 and B-02) and the resulting nanoparticle solution is collected in a round bottom flask (B-03). The microfluidic setup (Figure 10) is comparable to syntheses applied in literature.[57-59] Three syringe combinations were investigated (Table 2).

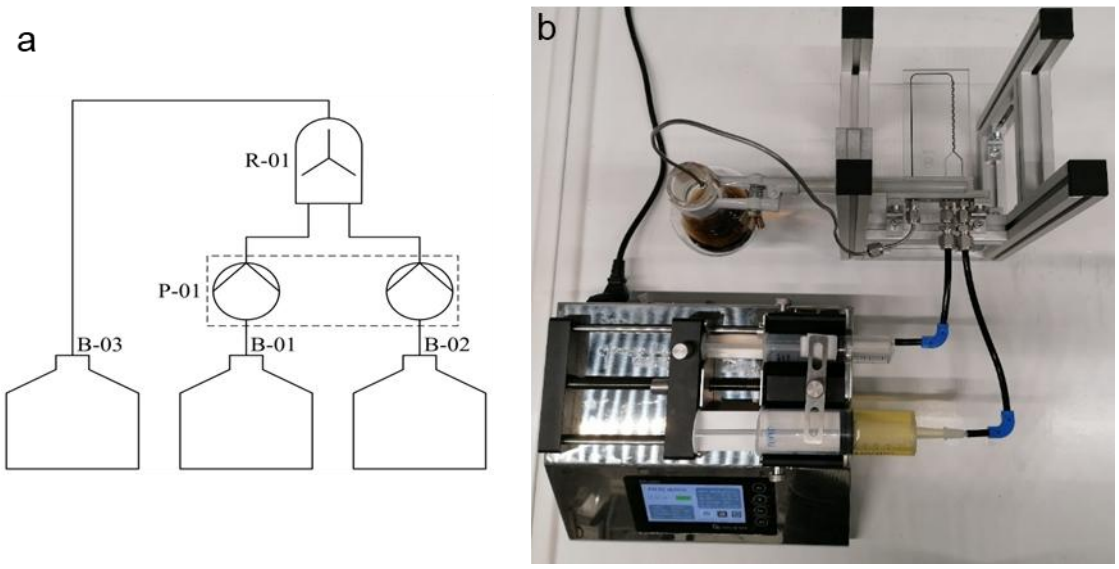

Figure 10: (a) Schematic illustration and (b) photograph of the laboratory setup for the continuous microfluidic synthesis of Pt nanoparticles.

Table 2: Investigated syringe combinations for the continuous synthesis of Pt nanoparticles. The large syringe is used for the Pt-PVP solution, the small syringe is used for the NaOH stabilized $NaBH_4$ solution.

Combination index	$V_{large\ syringe}$ [mL]	$L_{large\ syringe}$ [cm]	$V_{small\ syringe}$ [mL]	$L_{small\ syringe}$ [cm]	Flow rate ratio* [-]
A	30	11	20	9	1.54
B	30	11	10	7.5	3.57
C	100	13.5	30	9	6.50

* Flow rate ratio = (syringe diameter ratio)^2

Continuous nanoparticle syntheses were performed with the combinations A, B and C. Based on the findings from previous batch syntheses, the respective stock solutions were prepared with the PVP:Pt and $NaBH_4$:Pt ratios required to target platinum nanoparticles with a particle size of 2.4 nm (5 g_{PVP} g_{Pt}^{-1}, 0.47 mol_{NaBH4} mol_{Pt}^{-1}, 10 mM NaOH). According to literature, a flow rate of 0.84 mL min^{-1} was set for the Pt-PVP solution in the large syringe.[60] The platinum nanoparticles from the continuous syntheses with the different syringe combinations exhibit mean particle diameters of 2.66 (A), 2.69 (B) and 2.68 nm (C) according to analysis by means of HR-TEM (Figure S10), which are marginally higher than the targeted value of 2.4 nm (Figure 11). This may be an artefact of the broadened size distributions for continuously synthesized nanoparticles with standard deviations of ±0.45, ±0.48, and ±0.40 nm for the different combinations A, B, and C, respectively (±0.23nm for batch procedure). Since there is little difference in the particle sizes of the Pt nanoparticles produced via the different syringe combinations, combination C is selected due to the narrow particle size distribution in combination with the largest volume of nanoparticle suspension facilitating the scale-up of the synthesis procedure. The synthesis volume is twice as high as in the standardized batch synthesis, while the continuous synthesis may be easily scaled further.

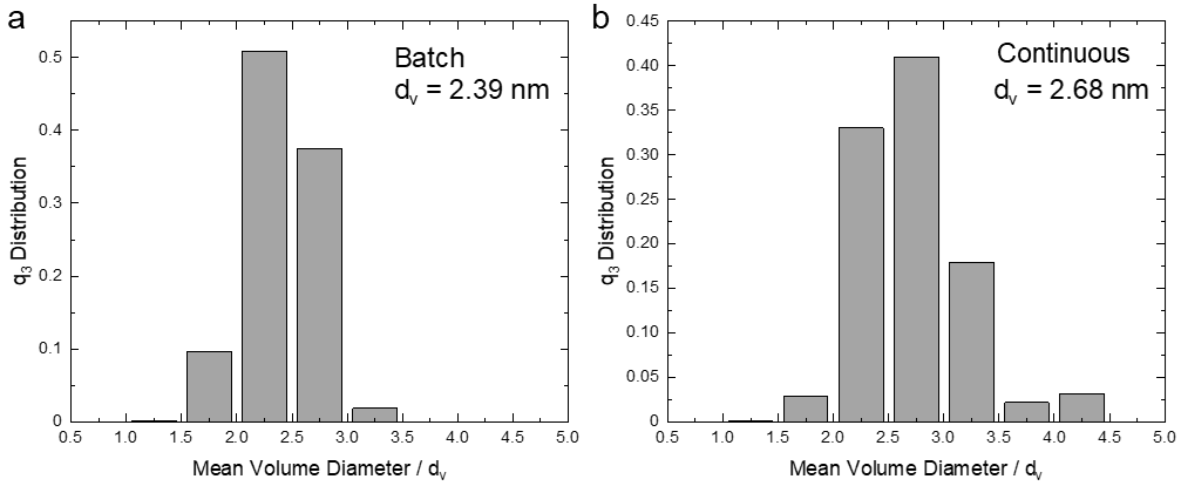

Figure 11: Pt nanoparticle size distributions for Pt/Al_2O_3 catalysts synthesized via (a) batch and (b) continuous procedure. Synthesis conditions: Batch procedure with PVP:Pt ratio = 5 g_{PVP} g_{Pt}^{-1}, $NaBH_4$:Pt ratio = 0.47 mol_{NaBH4} mol_{Pt}^{-1}, c_{NaOH} = 10 mM. Continuous procedure with syringe combination C, $F_{big\ syringe}$ = 0.84 mL min^{-1}, PVP:Pt ratio = 5 g_{PVP} $_{Pt}^{-1}$, $NaBH_4$:Pt ratio = 0.47 mol_{NaBH4} mol_{Pt}^{-1}, c_{NaOH} = 10 mM.

In order to achieve a defined Pt nanoparticle size, the influence of the amount of reducing agent on the Pt particle size was also investigated for the continuous process. For this purpose, several stock solutions with different concentrations of the reducing agent $NaBH_4$ were prepared and subsequently used in the continuous colloidal synthesis with chemical reduction. The general correlation between the $NaBH_4$:Pt ratio and the Pt nanoparticle size in the continuous synthesis is comparable to the batch synthesis (Figure S11), where the mean particle size of Pt nanoparticles synthesized continuously deviates marginally (~0.2-0.3 nm) from their equivalents of the batch route for the same $NaBH_4$:Pt ratio. Here, and in contrary to the batch synthesis, a plateau was reached at 2.8 nm for the continuous synthesis route (Figure 12). This emphasizes, in line with the previous findings in this work and of Van Rheenen *et al.*[54], that the maximum achievable particle size via the applied colloidal synthesis with basic $NaBH_4$ solutions at pH 12 and under ambient conditions lies around 2.8 nm, regardless of the operation mode of the synthesis.

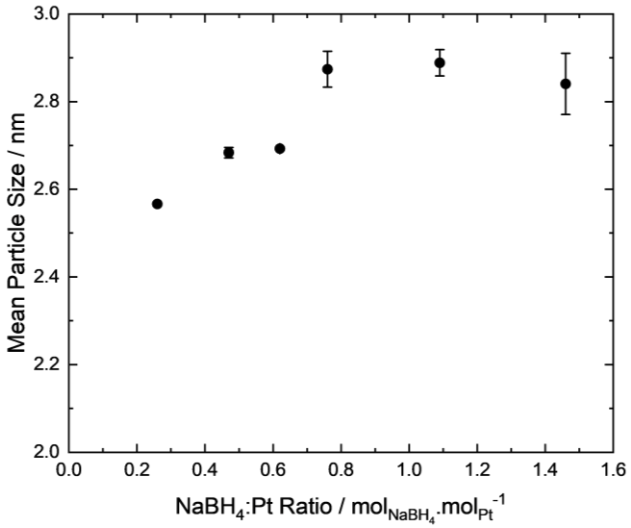

Figure 12: Influence of the specific amount of basic reducing agent $NaBH_4$ on the size of Pt nanoparticles from the continuous colloidal synthesis with chemical reduction. Synthesis conditions: Continuous procedure with syringe combination C (100 mL, 30 mL), $F_{big\ syringe}$ = 0.84 mL min^{-1}, PVP:Pt ratio = 5 g_{PVP} g_{Pt}^{-1}. Error bars represent standard deviation for three reproductions.

Lastly, the performance of the continuously synthesized Pt/Al_2O_3 catalysts in the dehydrogenation of H12-BT was evaluated at a reaction temperature of 230 °C (Figure 13).

The low reaction temperature was selected to amplify potential differences in the performance. A catalyst with the same particle size from the batch synthesis procedure is used as benchmark. Both catalysts show a similar performance indicating that the continuous synthesis route may be applied for the production of dehydrogenation catalysts and, apart from the slightly increased particle size, has no influence on the activity of the obtained catalysts.

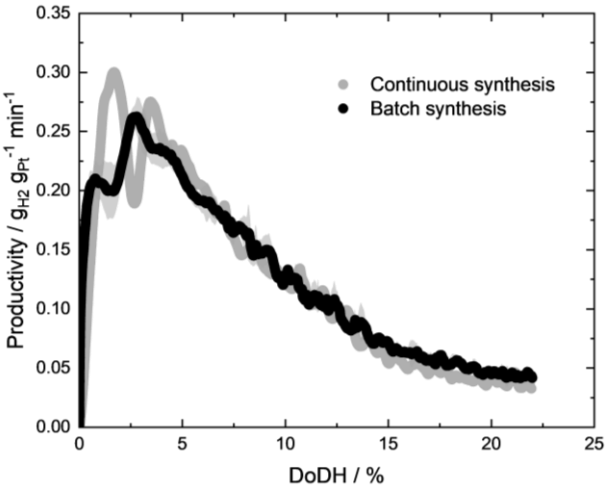

Figure 13: Productivity as a function of degree of dehydrogenation (DoDH) during semi-batch dehydrogenation of H12-BT using Pt/Al_2O_3 powder catalysts with platinum nanoparticle sizes of 2.4 nm synthesized via batch or continuous synthesis route. Reaction conditions: T = 230 °C, $n_{Pt}:n_{LOHC}$ = 0.001 mol.%, F_{Ar} = 300 mL min^{-1}, $t_{Reaction}$ = 120 min, Pt loading = 0.2 wt.%. Synthesis conditions: Batch or continuous procedure with powders, PVP:Pt ratio = 5 g_{PVP} g_{Pt}^{-1}, $NaBH_4$:Pt ratio = 0.31 mol_{NaBH4} mol_{Pt}^{-1}, C_{NaOH} = 10 mM.

Comparison of synthesis routes

The scope of this study is to investigate the synthesis of Pt/Al_2O_3 catalysts via the colloidal route and to establish a reproducible and scalable preparation route for well-defined dehydrogenation catalysts. The applied colloid chemical synthesis of nanoparticles is special since the reduction of the metal precursor, and hence the particle formation regime, may occur independent from the employed support.[61,62] The utilization of a chemical reducing agent is widely deployed in size-selective colloidal syntheses and facilitates good control over the quantity and strength of the reduction force, contrary to thermal treatment and reduction under hydrogen atmospheres. However, the latter is of equal importance, due to its scalability and applications in industry. As a result, this study evaluated the different parameters of the colloidal route, as well as attempted two scale-up steps to enable the synthesis of larger batches for e.g., studies in technical reactors. Several batch and continuous syntheses are presented covering a wide range of nanoparticle and batch sizes (Figure S14). In particular the continuous synthesis enables large batch sizes.

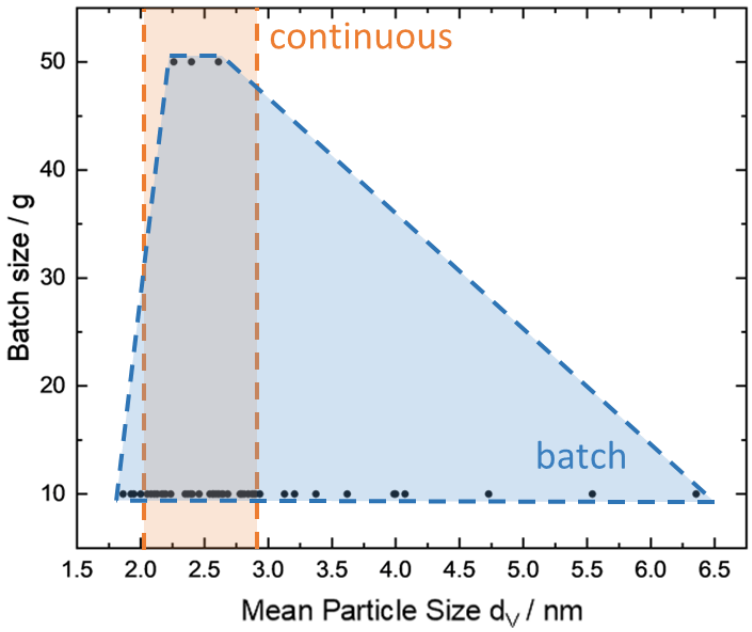

Figure 14: Batch and nanoparticle sizes covered by the presented batch (two batch sizes) and continuous (variable batch size) synthesis procedures.

The reducing agent, $NaBH_4$, was identified to have the largest influence on the herein used colloidal route and for the proposed catalyst system, whilst the role of PVP was only marginal in varying Pt nanoparticle size. Nonetheless, a more precise control over particle size was strived, which was established by inhibiting the hydrolysis of $NaBH_4$ via addition of NaOH and hence increasing the basicity towards a pH~12. Not only did this achieve more control over particle size, due to the controlled hydrolysis and hence variable reduction force, but it also increased the shelf-life of the reducing agent. Here, the half-life decay of the $NaBH_4$ solution increases from 9.1 min (aqueous solution) to 6.3 days at pH 12.[53-56] This serves as the foundation for the scale-up of this synthesis route, since the reduction occurs in a rather controlled manner in basic solutions than instanteneous for aqeous ones. However, utilizing basic $NaBH_4$ solutions demonstrates a limit for the achievable platinum paricle size at 2.8 nm (Figuree S11), corresponding to findings in the literature.[54] Moreover, the performance of catalysts with similar Pt particle sizes, synthesized using aqueous or basic $NaBH_4$ solutions, demonstrate no change in performance. This indicates that these catalysts can be used for dehydrogenation reactions, where C-H bondbreaking is involved, regardless of the type of reducing agent used. The nanoparticles prepared via a continuous microfluidic synthesis setup demonstrated comparable Pt particle sizes and performance in the dehydrogenation of H12-BT.

After establishing a foundation for controlling Pt particle size, the first shaped catalysts were produced to allow technical studies on structure sensitivity. Here, only marginal change in performance between shaped and powder catalysts is detected, possibly due to mass transport limitations accompanying the use of shaped supports. Thereafter, the first attempt for scaling up the amount of yielded catalyst to 50 g was conducted successfully, but had a detrimental effect on the dehydrogenation activity.

Finally, to assess the colloidal synthesis route itself and for comparison with classical catalyst preparation routes, the shaped catalysts of this study and the state-of-art industrial catalyst for the dehydrogenation of H12-BT and H18-DBT are compared in the dehydrogenation of H12-BT at 250 °C (Figure 15). Note, that the industrial catalyst is selectively poisoned with sulfur and has been optimized for operation at 310 °C.[35] Nonetheless, both catalysts demonstrate comparable performance over 2 h. Other catalyst systems in literature clearly outperform the presented catalysts due to a superior design, such as the addition of promoters or an optimized Pt nanoaprticle size.[13,63-64] In the herein presented catalysts, potential hindrance by residual PVP may represent another detrimental factor.

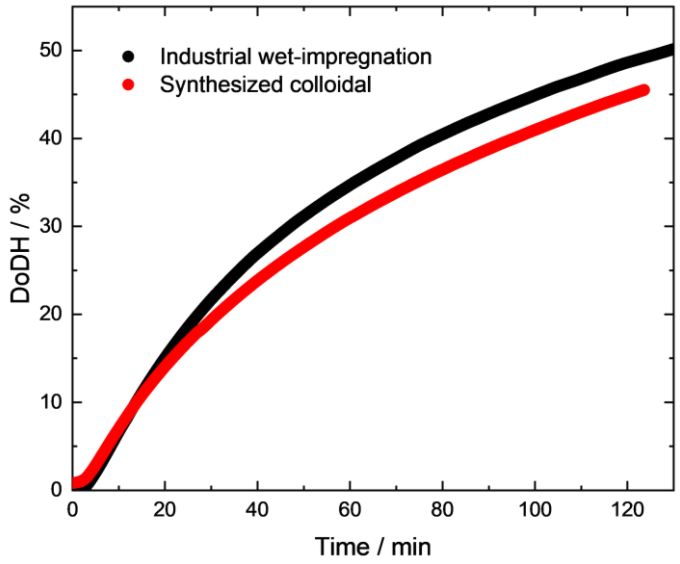

Figure 15: Degree of dehydrogenation of H12-BT over time at 250 °C for shaped Pt/Al_2O_3 catalysts synthesized via colloidal or wet-impregnation approach. Reaction conditions: T = 250 °C, $n_{Pt}:n_{LOHC}$ = 0.001 mol.%, F_{Ar} = 300 mL min^{-1}, $t_{Reaction}$ = 120 min, Pt loading = 0.2 wt.% Pt for synthesized catalysts; 0.3 wt.% Pt for industrial catalyst. Synthesis conditions: Batch procedure with shaped Al_2O_3, PVP:Pt ratio = 5 g_{PVP} g_{Pt}^{-1}, $NaBH_4$:Pt ratio = 0.31 mol_{NaBH4} mol_{Pt}^{-1}.

Summary and conclusions

In this work, a colloidal approach in combination with chemical reduction was optimized for the synthesis of well-defined Pt nanoparticles focusing on size control. After immobilization onto Al_2O_3 support materials, the supported catalysts were employed in the dehydrogenation of the LOHC H12-BT without further pre-treatment. Different parameters were varied during the synthesis to evaluate their influence on the size of the Pt nanoparticles. The amount of the steric stabilizer PVP showed only a marginal effect on the platinum particle size for the studied range of PVP:Pt ratios. To minimize its potential effect on catalysis, the lowest ratio of 5 g_{PVP} g_{Pt}^{-1} was used. Similarly, the influence of the reducing agent $NaBH_4$ on Pt nanoparticle size was investigated. Supported nanoparticles in the size range of 2.0 to 6.0 nm were synthesized, while the amount of reducing agent scales with the nanoparticle size in agreement with theoretical models of particle formation. The use of basic $NaBH_4$ solutions allows for a more precise control of the Pt nanoparticle size up to 2.8 nm, while increasing the temporal stability of the reduction solution enabling its use in continuous synthesis. To provide well-defined catalysts for studies in technical reactors, the immobilization of the prepared Pt nanoparticles was transferred from powder to shaped supports by using hollow Al_2O_3 cylinders. Despite possible limitations due to mass transport effects during dehydrogenation of H12-BT as model reaction, the shaped catalysts showed only minor differences in catalytic performance compared to powder catalysts and was demonstrated with a scale-up yielding more than 50 g of well-defined Pt/Al_2O_3 catalyst in one step. Finally, the continuous synthesis of Pt nanoparticles using a microfluidic reactor was demonstrated and enables production of even larger quantities. Analogous to the observations from batch syntheses, the size of the Pt nanoparticles in the continuous syntheses was also mainly linked to the amount of reducing agent. Catalysts synthesized via the continuous procedure showed similar catalytic performance in the dehydrogenation of H12-BT as a comparable catalyst from batch synthesis.

Acknowledgments

Financial support by the Bavarian Ministry of Economic Affairs, Regional Development and Energy through the project “Emissionsfreier und stark emissionsreduzierter Bahnverkehr auf nicht-elektrifizierten Strecken” and by the Helmholtz Research Program “Materials and Technologies for the Energy Transition (MTET), Topic 3: Chemical Energy Carriers” is highly

acknowledged. Infrastructural support by DFG via its SFB 1452 (Catalysis at Liquid Interfaces, CLINT) is also gratefully acknowledged.

Conflicts of interest

Peter Wasserscheid is the co-founder and minority shareholder of Hydrogenious LOHC Technologies GmbH, Erlangen, a company that has commercialised equipment for hydrogen storage using the LOHC technology.

Additional note

Part of the herein presented results were published in the doctoral thesis of the first author Dr. Yazan Mahayni,[65] which was submitted to the University of Erlangen–Nuremberg in 2023.

References

[1] A. Le Valant, C. Comminges, F. Can, K. Thomas, M. Houalla, F. Epron, *The Journal of Physical Chemistry C* **2016**, *120*, 26374-26385.
[2] F. Auer, A. Hupfer, A. Bösmann, N. Szesni, P. Wasserscheidpeter, *Catalysis Science & Technology* **2020**, *10*, 6669-6678.
[3] G. A. Somorjai, J. Carrazza, *Industrial & Engineering Chemistry Fundamentals* **1986**, *25*, 63-69.
[4] H. Lee, S. E. Habas, S. Kweskin, D. Butcher, G. A. Somorjai, P. Yang, *Angewandte Chemie International Edition* **2006**, *45*, 7824-7828.
[5] G. A. Somorjai, Y. Li, *Introduction to surface chemistry and catalysis*, Wiley, Hoboken (New Jersey), **2010**.
[6] K. G. Papanikolaou, M. Stamatakis, *Catalysis Science & Technology* **2020**, *10*, 5815-5828.
[7] R. K. Herz, W. D. Gillespie, E. E. Petersen, G. A. Somorjai, *Journal of Catalysis* **1981**, *67*, 371-386.
[8] S. M. Davis, G. A. Somorjai, *Journal of Catalysis* **1980**, *65*, 78-83.
[9] G. A. Somorjai, D. W. Blakely, *Nature* **1975**, *258*, 580-583.
[10] M. R. Usman, *Kinetics of Methylcyclohexane Dehydrogenation and Reactor Simulation for "On-board" Hydrogen Storage*, Doctoral Thesis, Universtiy of Manchester **2010**.
[11] B. A. T. Mehrabadi, S. Eskandari, U. Khan, R. D. White, J. R. Regalbuto, **2017**, pp. 1-35.
[12] C. Perego, P. Villa, *Catalysis Today* **1997**, *34*, 281-305.
[13] D. Strauch, P. Weiner, B. B. Sarma, A. Körner, E. Herzinger, P. Wolf, A. Zimina, A. Hutzler, D. E. Doronkin, J.-D. Grunwaldt, P. Wasserscheid, M. Wolf, *Catalysis Science & Technology* **2024**, *14*, 1775-1790.
[14] S. Kaneko, M. Izuka, A. Takahashi, M. Ohshima, H. Kurokawa, H. Miura, *Applied Catalysis A: General* **2012**, *427-428*, 85-91.

[15] O. S. Alexeev, S. Y. Chin, M. H. Engelhard, L. Ortiz-Soto, M. D. Amiridis, *The Journal of Physical Chemistry B* **2005**, *109*, 23430-23443.
[16] A. Goguet, D. Schweich, J. P. Candy, *Journal of Catalysis* **2003**, *220*, 280-290.
[17] J. T. Miller, M. Schreier, A. J. Kropf, J. R. Regalbuto, *Journal of Catalysis* **2004**, *225*, 203-212.
[18] M. K. Oudenhuijzen, P. J. Kooyman, B. Tappel, J. A. van Bokhoven, D. C. Koningsberger, *Journal of Catalysis* **2002**, *205*, 135-146.
[19] D. Zakgeym, T. Engl, Y. Mahayni, K. Müller, M. Wolf, P. Wasserscheid, *Applied Catalysis A: General* **2022**, *639*, 118644.
[20] J. T. Miller, M. Schreier, A. J. Kropf, J. R. Regalbuto, *Journal of Catalysis* **2004**, *225*, 203-212.
[21] J. A. Moulijn, A. E. van Diepen, F. Kapteijn, *Applied Catalysis A: General* **2001**, *212*, 3-16.
[22] H. Nagao, M. Ichiji, I. Hirasawa, *Chemical Engineering & Technology* **2017**, *40*, 1242-1246.
[23] S. C. Jung, S. W. Nahm, H. Y. Jung, Y. K. Park, S. G. Seo, S. C. Kim, *Journal of Nanoscience & Nanotechnology* **2015**, *15*, 5461-5465.
[24] S. A. Gama-Lara, R. A. Morales-Luckie, L. Argueta-Figueroa, J. P. Hinestroza, I. García-Orozco, R. Natividad, *Journal of Nanomaterials* **2018**, *2018*, 1-8.
[25] D. Pham Minh, Y. Oudart, B. Baubet, C. Verdon, C. Thomazeau, *Oil & Gas Science and Technology - Revue de l'IFP* **2009**, *64*, 697-706.
[26] S. Kidambi, J. Dai, J. Li, M. L. Bruening, *Journal of the American Chemical Society* **2004**, *126*, 2658-2659.
[27] M. Liu, W. Yu, H. Liu, *Journal of Molecular Catalysis A: Chemical* **1999**, *138*, 295-303.
[28] K. Mavani, M. Shah, *International Journal of Engineering Research & Technology (IJERT)* **2013**, *2*, IJERTV2IS3605.
[29] H. Hiramatsu, F. E. Osterloh, *Chemistry of Materials* **2004**, *16*, 2509-2511.
[30] I. Hussain, S. Graham, Z. Wang, B. Tan, D. C. Sherrington, S. P. Rannard, A. I. Cooper, M. Brust, *Journal of the American Chemical Society* **2005**, *127*, 16398-16399.
[31] X. Zeng, B. Zhou, Y. Gao, C. Wang, S. Li, C. Y. Yeung, W. Wen, *Nanotechnology* **2014**, *25*, 495601.
[32] B. A. Mehrabadi, S. Eskandari, U. Khan, R. D. White, J. R. Regalbuto, *Advances in Catalysis* **2017**, *61*, 1-35.
[33] M. Willer, P. Preuster, M. Geißelbrecht, P. Wasserscheid, *International Journal of Hydrogen Energy* **2024**, *57*, 1513-1523.
[34] J. Kadar, F. Gackstatter, F. Ortner, L. Wagner, M. Willer, P. Preuster, P. Wasserscheid, M. Geißelbrecht, *International Journal of Hydrogen Energy* **2024**, *59*, 1376-1387.
[35] N. Szesni, F. Frankl, S. Sturm, P. Wasserscheid, A. Seidel and A. Boesmann, US20210077984A1, *Platinum-sulfur-based shell catalyst, production and use thereof in the dehydrogenation of hydrocarbons*, **2021**.
[36] F. Auer, D. Blaumeiser, T. Bauer, A. Bösmann, N. Szesni, J. Libuda and P. Wasserscheid, *Catalysis Science & Technology* **2019**, *9*, 3537.
[37] M. Geißelbrecht, S. Mrusek, K. Müller, P. Preuster, A. Bösmann, P. Wasserscheid, *Energy & Environmental Science* **2020**, *13*, 3119-3128.
[38] T. Rüde, S. Dürr, P. Preuster, M. Wolf, P. Wasserscheid, *Sustainable Energy & Fuels* **2022**, *6*, 1541-1553.
[39] T. Teranishi, M. Hosoe, T. Tanaka, M. Miyake, *The Journal of Physical Chemistry B* **1999**, *103*, 3818-3827.

[40] Rohm and Haas, Eds., *Sodium borohydride digest*. Rohm and Haas Company. *Synthesis & Process Applications*, **2003**.
[41] R. Retnamma, C. Rangel, A. Q. Novais, M. A. Matthews, *Kinetics of Sodium Borohydride Hydrolysis in Aqueous-basic Solutions*, in *HYCELTEC'2013-IV Iberian Symposium on Hydrogen, Fuel Cells and Advanced Batteries*, **2013**.
[42] J. Polte, X. Tuaev, M. Wuithschick, A. Fischer, A. F. Thuenemann, K. Rademann, R. Kraehnert, F. Emmerling, *ACS Nano* **2012**, *6*, 5791-5802.
[43] J. Schindelin, C. T. Rueden, M. C. Hiner, K. W. Eliceiri, *Molecular Reproduction and Development* **2015**, *82*, 518-529.
[44] Sasol Germany GmbH, *PURALOX®/CATALOX® High purity activated aluminas*, https://sasoltechdata.com/tds/aluclox.pdf (accessed 15.10.2024).
[45] J. E. Newton, J. A. Preece, N. V. Rees, S. L. Horswell, *Physical Chemistry Chemical Physics* **2014**, *16*, 11435-11446.
[46] W. Huang, Q. Hua, T. Cao, *Catalysis Letters* **2014**, *144*, 1355.
[47] M. Wolf, N. Fischer, M. Claeys, *Materials Chemistry and Physics* **2018**, *213*, 305-312.
[48] V. K. LaMer, R. H. Dinegar, *Journal of the American Chemical Society* **1950**, *72*, 4847-4854.
[49] N. T. Thanh, N. Maclean, S. Mahiddine, *Chemical Reviews* **2014**, *114*, 7610-7630.
[50] J. Bedia, J. Lemus, L. Calvo, J. J. Rodriguez, M. A. Gilarranz, *Colloids and Surfaces A: Physicochemical and Engineering Aspects* **2017**, *525*, 77-84.
[51] J. M. M. Tengco, *Synthesis of Well Dispersed Supported Metal Catalysts by Strong Electrostatic Adsorption and Electroless Deposition*, Doctoral Thesis, University of South Carolina **2016**.
[52] W. Peters, A. Seidel, S. Herzog, A. Bösmann, W. Schwieger, P. Wasserscheid, *Energy & Environmental Science* **2015**, *8*, 3013-3021.
[53] R. E. Davis, C. G. Swain, *Journal of the American Chemical Society* **1960**, *82*, 5949-5950.
[54] P. R. Van Rheenen, M. J. McKelvy, W. S. Glaunsinger, *Journal of Solid State Chemistry* **1987**, *67*, 151-169.
[55] V. S. K. K. N. Mochalov, G. G. Gil'manshin, *Doklady Akademii Nauk SSSR* **1965**, *162*, 613-616.
[56] S. Nishimura, A. Takagaki, S. Maenosono, K. Ebitani, *Langmuir* **2010**, *26*, 4473-4479.
[57] S. Marre, K. F. Jensen, *Chemical Society Reviews* **2010**, *39*, 1183-1202.
[58] G. Tofighi, H. Lichtenberg, J. Pesek, T. L. Sheppard, W. Wang, L. Schöttner, G. Rinke, R. Dittmeyer, J.-D. Grunwaldt, *Reaction Chemistry & Engineering* **2017**, *2*, 876-884.
[59] G. Tofighi, H. Lichtenberg, A. Gaur, W. Wang, S. Wild, K. Herrera Delgado, S. Pitter, R. Dittmeyer, J.-D. Grunwaldt, D. E. Doronkin, *Reaction Chemistry & Engineering* **2022**, *7*, 730-740.
[60] P. L. Suryawanshi, S. P. Gumfekar, P. R. Kumar, B. B. Kale, S. H. Sonawane, *Colloid and Interface Science Communications* **2016**, *13*, 6-9.
[61] D. D. Evanoff, G. Chumanov, *The Journal of Physical Chemistry B* **2004**, 108, 13957-13962.
[62] Y. Zhao, J. Baeza, N. K. Rao, L. Calvo, M. Gilarranz, Y. Li, L. Lefferts, *Journal of Catalysis* **2014**, 318, 162-169.
[63] K. Alconada, V.L. Barrio, *International Journal of Hydrogen Energy* **2024**, 51, 243-255.
[64] J. K. Yoo, S.-H. Lee, T. I. Park, J. H. Lee, K.-Y. Lee, *ACS Catalysis* **2025**, 15, 114-128.
[65] Y. Mahayni, Doctoral Dissertation, **2023**, Friedrich-Alexander-Universität Erlangen Nürnberg, https://open.fau.de/handle/openfau/23905.